Sensors and Materials, Vol. 34, No. 2 (2022) 789–801
MYU Tokyo

S & M 2853

Machine-vision-based Spindle Positioning System of Grinding-wheel-saw Automatic Replacement System

Sijie Qiu,[1] Chi-Hsin Yang,[1*] Long Wu,[1] Kun-Chieh Wang,[1] and Jian-Zhou Pan[2]

[1]School of Mechanical and Electric Engineering, Sanming University, Sanming, Fujian Province 365004, China
[2]Fujian Sansteel (Group) Co. Ltd., Sanming, Fujian Province 365004, China

(Received September 6, 2021; accepted December 20, 2021)

Keywords: machine vision, automatic replacement, spindle positioning, template matching

To improve the working efficiency and safety of steel round bar sawing equipment, a grinding-wheel-saw automatic replacement system has been employed to replace grinding-wheel saws. In this paper, we report a machine-vision-based spindle positioning system for spindle localization in this replacement system. The hardware and software for the spindle positioning system were established, as well as an imaging model of the camera and the calibration of the vision system. The template matching approach applied to identify the shaft nut of the spindle is also described. Experimental results clearly demonstrate the effectiveness of the proposed machine-vision-based system.

1. Introduction

In recent years, owing to the rapid development of image processing technology and the cost reduction of related hardware and software, machine-vision detection has been widely applied in various fields, for example, identification of the center position of water chamber drain holes for nuclear power steam generators,(1) metro tunnel deformation,(2) grinding-wheel condition monitoring,(3) geometric parameter measurement for rivet thin plates,(4) and circle detection of printed circuit boards (PCBs).(5) In addition, many kinds of machine-vision-based equipment have also been developed.(6–10) In Ref. 7, vision-based initial point alignment control was presented for the wheel hubs in a robotic polishing system. In Ref. 8, a motion controller developed by machine vision for a knuckle boom crane with cable length estimation was reported to achieve a high performance. In Ref. 9, a computer-vision-based intelligent harvesting system with a deep learning algorithm was developed to detect the level of maturity of dates.

Steel products, such as hot-rolled steel plates, cold-rolled strips, and steel round bars, have many important industrial uses. Steel round bars are the main product of steelworks. According to the requirements of customers, the produced steel round bars must be cut to a standard length. In the past, steel round bars were directly cut by a general cutting machine at room temperature. However, the employed process resulted in serious quality problems at the end of round bars such as a horseshoe cross section. Moreover, burrs on the end section and cracking on the shear end also directly affected the yield rate of products. To improve the quality of products and their

*Corresponding author: e-mail: 20190207@fjsmu.edu.cn
https://doi.org/10.18494/SAM3638

ISSN 0914-4935
https://myukk.org/

specifications, a huge sawing machine, as shown in Fig. 1, has been utilized to saw steel round bars at a suitable operating temperature. At present, grinding-wheel machines with a machine-vision detection system are mainly applied to polish the rough surface of manufactured workpieces,[3,7] and grinding-wheel equipment with machine-vision parts for sawing has seldom been set up. The novelty of this paper is the establishment of a machine-vision-based spindle positioning system suitable for grinding-wheel-saw equipment.

The installed grinding-wheel saw in the steel round bar sawing equipment has a mass of 50 kg and a diameter of 1250 mm. Owing to the high frequency of usage and the rapid wear, the grinding-wheel saw must be replaced frequently. However, a workshop may have a harsh environment including a high temperature, dust, and limited space, resulting in a major reduction in efficiency as a result of manual grinding-wheel-saw replacement and a high cost.

To reduce the problems associated with the manual replacement of grinding-wheel saws for steel round bar sawing equipment, a machine-vision-based grinding-wheel-saw automatic replacement system was set up. The system for detecting the spindle location for this automatic replacement equipment is the key issue. The contribution of this work is to develop a machine-vision-based spindle positioning system by utilizing the architecture of a digital camera attached on the end-effector of an industrial robot arm. The hardware and software of the machine vision system for detecting the spindle location are proposed, which are based on the principle of eye-in-hand machine vision and template matching technology. The established automatic replacement system with a machine-vision-based spindle positioning system effectively improved the working efficiency and safety of the steel round bar sawing equipment and reduced the operating cost.

The rest of this paper is organized as follows. In Sect. 2, the configuration of the grinding-wheel-saw automatic replacement system is introduced. The operations of the automatic system are also described. The setup of the machine-vision-based spindle positioning system for the grinding-wheel-saw automatic replacement system is presented in Sect. 3. The imaging model

Fig. 1. (Color online) Grinding-wheel-saw equipment for sawing process.

and calibration of the vision system and the template matching approach for spindle localization are reported in Sects. 4 and 5, respectively. Finally, concluding remarks are made.

2. Configuration of Grinding-wheel-saw Automatic Replacement System

Figure 2 shows the framework of the machine-vision-based automatic replacement system developed to replace the grinding-wheel saws for steel round bar sawing equipment. The system mainly comprises two parts, a tightening and disassembly manipulator with six degrees of freedom (6DOF) and a six-axis industry robot arm with a vacuum extraction mechanism, as depicted in Fig. 3. They are applied to complete the tasks of disassembly and tightening, and the replacement of the grinding-wheel saw, respectively. The 6DOF tightening and disassembly manipulator with a pneumatic wrench system is used for disassembly and assembly of the hexagonal shaft nut and the positioning flange of the grinding-wheel saw. The six-axis industrial robot arm with a vacuum extraction mechanism and a digital camera mounted on the end-effector is applied to extract and replace the old grinding-wheel saw. The operation of the machine-vision-based grinding-wheel-saw automatic replacement system has the following five steps.

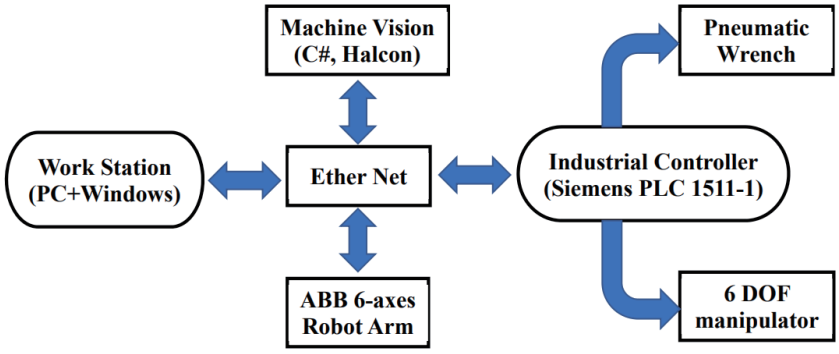

Fig. 2. (Color online) Framework of machine-vision-based grinding-wheel-saw automatic replacement system.

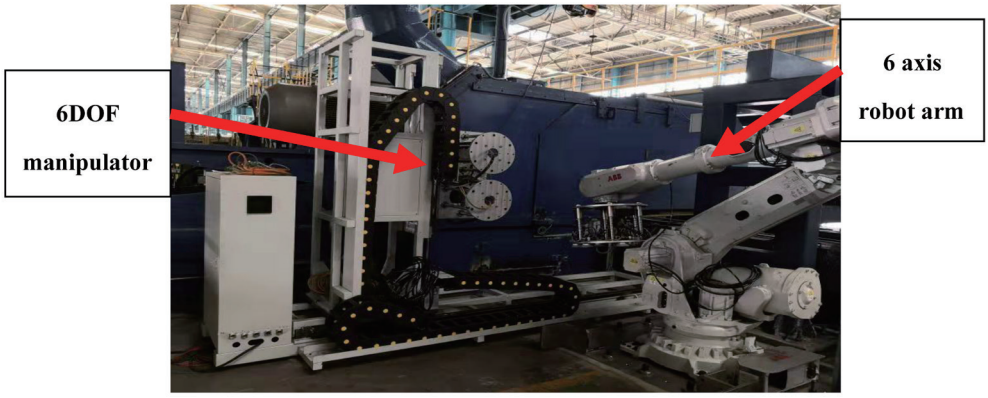

Fig. 3. (Color online) Machine-vision-based grinding-wheel-saw automatic replacement system.

(1) Machine vision positioning is carried out by the eye-in-hand digital camera to locate the center position of the shaft nut of the spindle for the old grinding-wheel saw.
(2) The 6DOF tightening and disassembly manipulator is disassembled to extract the hexagonal shaft nut of the grinding-wheel saw. Then the positioning flange is extracted.
(3) The six-axis industrial robot arm in the automatic replacement system is operated to absorb the old grinding-wheel saw and place it where the discarded saws are stored.
(4) Machine vision positioning is used again to locate the positions where new grinding-wheel saws are stored. The six-axis industrial robot arm takes a new saw and places it on the spindle of the grinding-wheel saw.
(5) The 6DOF tightening and disassembly manipulator is operated again to install the positioning flange and the hexagonal shaft nut on the spindle in sequence. Finally, the hexagonal shaft nut is tightened by the pneumatic wrench system.

In the aforementioned steps, the detection of the spindle location is the key point in the automatic replacement system. In this work, to detect the spindle location, a machine-vision-based spindle positioning system is developed, as described in the following.

3. Setup of the Machine-vision-based Spindle Positioning System

The machine-vision-based spindle positioning system for the round bar sawing equipment mainly comprises a hardware system and a software part. The key parts of the overall system are listed in Table 1. The main goal of the hardware system is to acquire clear images of the hexagonal shaft nut on the spindle. The software part mainly uses the developed algorithm to evaluate the image coordinates of the grinding-wheel-saw shaft nut of the spindle and transforms the image coordinates into real-world coordinates according to the vision system calibration. Moreover, motion planning commands of the robot arm according to the results of machine-vision detection are also proposed.

The hardware system is mainly composed of the industrial camera with a dedicated lens, the light source, and the ABB IRB6700-150 six-axis robot arm. The camera of the image acquisition device is a HIKROBOT MV-CA020-20GM 2.0 MP 2/3″ CMOS monochrome GigE camera. Its resolution is 1920 × 1200 and its frame rate is 54 fps. The dedicated lens is a HIKROBOT MVL-HF1628M-6MP 1/1.8″ 12 mm F2.8 Manual Iris C-Mount lens with a rating of 6 megapixels and a minimum object distance of 0.06 m. The light source of the integrated annular lighting system

Table 1
Key parts of machine-vision-based spindle positioning system.

No.	Item	Model	Specifications
1	Camera	MV-CA020-20GM	Resolution: 200 megapixels
2	Lens	MVL-HF1628M-6MP	Focal length: 16 mm
3	Light source	Annular lighting system	Tuning white light: 220 V, 60 W
4	Robot arm	ABB IRB6700-150	Maximum load: 150 kg
5	Environment of developed system	VS2019, Windows	System integrating interface design
6	Machine vision library	MVTec HALCON 18.11	Algorithms of machine vision
7	Motion planning of robot arm	ABB RobotStudio 6.08	Motion programming

is a 220 V, 60 W LED. The digital camera with the lens is mounted on the end-effector of the six-axis robot arm and moves with the robot arm. The software part is developed in the VS2019 environment based on the Windows operation system installed in an industrial personal computer. The related machine-vision algorithms are programmed in C# language with the MVTec HALCON 18.11 machine-vision library. The motion planning of the robot arm is built in the ABB RobotStudio 6.08 compilation environment.

4. Pinhole Imaging Model of Camera

The detection and motion planning of the six-axis robot arm are based on machine-vision technology. The imaging model and calibration of the vision system are introduced in the following.

4.1 Derivation of model

In the work, a pinhole imaging model is applied to the camera imaging model. Figure 4 shows a schematic diagram of the model.[11] The transformation relationship between the image frame coordinates (x, y) and the camera frame coordinates (X_C, Y_C, Z_C) is expressed by[11–14]

$$\begin{bmatrix} x \\ y \\ 1 \end{bmatrix} = \frac{1}{Z_C} \begin{bmatrix} f & 0 & 0 & 0 \\ 0 & f & 0 & 0 \\ 0 & 0 & 1 & 0 \end{bmatrix} \begin{bmatrix} X_C \\ Y_C \\ Z_C \\ 1 \end{bmatrix}, \tag{1}$$

where f is the focal length of the camera and (x, y) and (X_C, Y_C, Z_C) are the image frame and camera frame coordinates, respectively. In accordance with Fig. 5, the transformation between the image frame coordinates (x, y) and the image pixel coordinates (u, v) is obtained. The transformed matrix is as follows:

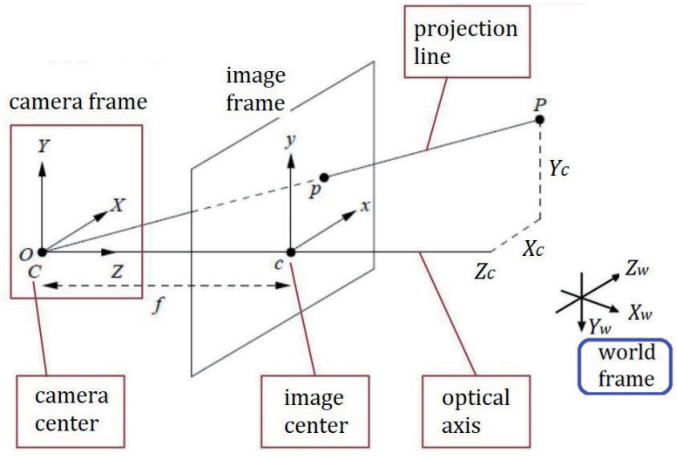

Fig. 4. (Color online) Schematic diagram of the pinhole imaging model.

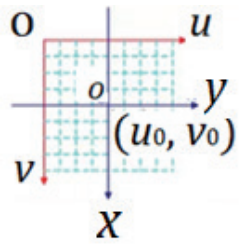

Fig. 5. (Color online) Relation between image frame coordinates (x, y) and image pixel coordinates (u, v).

$$\begin{bmatrix} u \\ v \\ 1 \end{bmatrix} = \begin{bmatrix} 1/dx & 0 & u_0 \\ 0 & 1/dx & v_0 \\ 0 & 0 & 1 \end{bmatrix} \begin{bmatrix} x \\ y \\ 1 \end{bmatrix}, \tag{2}$$

where (u_0, v_0) are the coordinates of the primary point, and dx and dy represent the shrinkage of pixels per unit length in the (u, v) directions, respectively. It is assumed that $\boldsymbol{R}$ is a rational matrix and $\boldsymbol{T}$ is the translational vector from the camera frame (X_C, Y_C, Z_C) to the world frame (X_W, Y_W, Z_W). The homogeneous transformation is represented by

$$\begin{bmatrix} R & T \\ 0^T & 1 \end{bmatrix} \equiv \left[R \middle| T \right]. \tag{3}$$

According to Eqs. (1)–(3), the transformation between the world coordinates (X_W, Y_W, Z_W) and the image pixel coordinates (u, v) can be given by

$$\begin{bmatrix} u & v & 1 \end{bmatrix}^T = P \begin{bmatrix} X_W & Y_W & Z_W & 1 \end{bmatrix}^T \tag{4}$$

$$P = \frac{1}{Z_C} \begin{bmatrix} 1/dx & 0 & u_0 \\ 0 & 1/dx & v_0 \\ 0 & 0 & 1 \end{bmatrix} \begin{bmatrix} f & 0 & 0 & 0 \\ 0 & f & 0 & 0 \\ 0 & 0 & 1 & 0 \end{bmatrix} \left[R \middle| T \right]. \tag{5}$$

$\boldsymbol{P}$ is a 3 × 4 matrix that includes the intrinsic parameters and pose parameters of the camera model. Moreover, it is the projection matrix from the image pixel coordinate system to the world coordinate system. The intrinsic parameters and pose parameters for the camera model were determined by the calibration technology.[15–17]

The least-squares approach was applied to find a suitable solution using Eqs. (4) and (5).[18–21] However, the distortion of the camera lens was not taken into account. To eliminate lens distortion, a camera calibration method based on a 2D plane target was employed.[22–24] In the proposed method, only a planar checkerboard calibration board is required, and the specific motion parameters of the calibration board are not required. During the calibration process, more than two pictures of the calibration board are taken by the camera.[23]

Owing to the application of a planar checkerboard calibration board, without loss of generality, it is assumed that the model plane is $Z_W = 0$ in the world coordinate system. The homogeneous transform, denoted by the homography matrix $\boldsymbol{H}$, which depends on the relative positions of the camera and the plane of the calibration board, and the camera's intrinsic parameters, can be derived from the 3 × 4 projection matrix $\boldsymbol{P}$ by setting the third column to the zero vector, $\vec{r}_3 = 0$ in the rational matrix $R = [\vec{r}_1 \quad \vec{r}_2 \quad \vec{r}_3]$.[23]

$$[u \quad v \quad 1]^T = P[X_W \quad Y_W \quad 0 \quad 1]^T \Rightarrow [X_W \quad Y_W \quad 1]^T = H[u \quad v \quad 1]^T \tag{6}$$

Here, the homography matrix $\boldsymbol{H}$ is a 3 × 3 matrix represented by

$$H = \begin{bmatrix} h_{11} & h_{12} & h_{13} \\ h_{21} & h_{22} & h_{23} \\ h_{31} & h_{32} & h_{33} \end{bmatrix}, \; h_{33} = 1. \tag{7}$$

For a given pair of coordinates (u_1, v_1) and (X_{W_1}, Y_{W_1}) of the image pixel and the world frame, respectively, the following linear equations are derived from Eqs. (6) and (7):

$$\begin{bmatrix} u_1 & v_1 & 1 & 0 & 0 & 0 & -u_1 X_{W_1} & -v_1 X_{W_1} \\ 0 & 0 & 0 & u_1 & v_1 & 1 & -u_1 Y_{W_1} & -v_1 Y_{W_1} \end{bmatrix} \boldsymbol{h} = \begin{bmatrix} X_{W_1} \\ Y_{W_1} \end{bmatrix}, \tag{8}$$

for vector $\boldsymbol{h} = [h_{11} \quad h_{12} \quad h_{13} \quad h_{21} \quad h_{22} \quad h_{23} \quad h_{31} \quad h_{32}]^T$. For $n \geq 4$ pairs of image pixel coordinates and world frame coordinates, the completely determined homography matrix $\boldsymbol{H}$ is obtained. Equation (8) with $n \geq 4$ pairs of coordinates yields

$$\begin{bmatrix} u_1 & v_1 & 1 & 0 & 0 & 0 & -u_1 X_{W_1} & -v_1 X_{W_1} \\ 0 & 0 & 0 & u_1 & v_1 & 1 & -u_1 Y_{W_1} & -v_1 Y_{W_1} \\ \vdots & \vdots & \vdots & \vdots & \vdots & \vdots & \vdots & \vdots \\ u_n & v_n & 1 & 0 & 0 & 0 & -u_n X_{W_n} & -v_n X_{W_n} \\ 0 & 0 & 0 & u_n & v_n & 1 & -u_n Y_{W_n} & -v_n Y_{W_n} \end{bmatrix} \boldsymbol{h} = \begin{bmatrix} X_{W_1} \\ Y_{W_1} \\ \vdots \\ X_{W_n} \\ Y_{W_n} \end{bmatrix} \Rightarrow B\boldsymbol{h} = A. \tag{9}$$

The vector $\boldsymbol{h} = [h_{11} \quad h_{12} \quad h_{13} \quad h_{21} \quad h_{22} \quad h_{23} \quad h_{31} \quad h_{32}]^T$ is solved by the least-squares method[18–21] as

$$\boldsymbol{h} = (B^T B)^{-1} B^T A. \tag{10}$$

By solving the vector $\boldsymbol{h}$, the homography matrix $\boldsymbol{H}$ is obtained. The one-to-one transformation between the image plane and the world frame is thus determined.

4.2 Experimental results for calibration

The prototype calibration system of the machine-vision-based spindle positioning system for the grinding-wheel-saw automatic replacement system is shown in Fig. 6. The industrial camera is mounted on the end-effector of the six-axis industrial robot arm. The world coordinate (X_W, Y_W, Z_W) system is attached on the fixed base of the robot arm. The calibration target is the calibration board on the grinding-wheel saw, and the Z_W axis of the world frame is perpendicular to the plane of the saw and oriented outward. In the calibration experiments, Z_W, the axis height, and the rotation angle of the camera on the six-axis robot are fixed.

The experimental pairs of coordinates of the image pixel (u, v) and world frame (X_W, Y_W) are used for the calibration. To move the robot arm $n \geq 4$ times and record the data in the (X_W, Y_W) plane, the pairs of image pixel coordinates and world frame coordinates are obtained by the established software. The software interface is shown in Fig. 7. In this study, nine movements of the robot arm are performed, and the nine pairs of coordinates used as data for calibration are listed in Table 2.

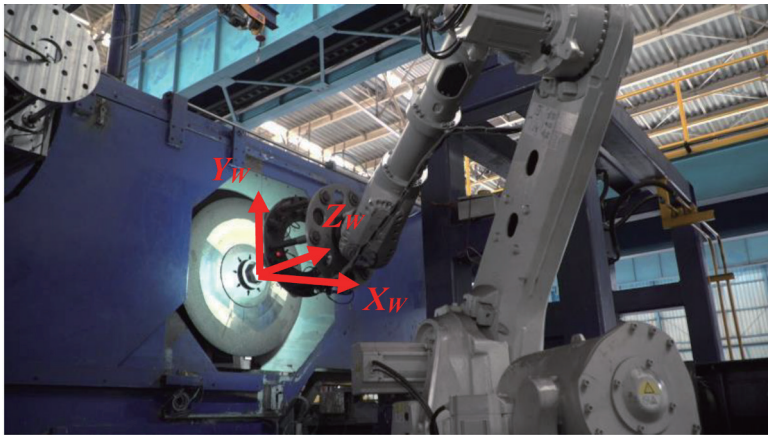

Fig. 6. (Color online) Prototype calibration system.

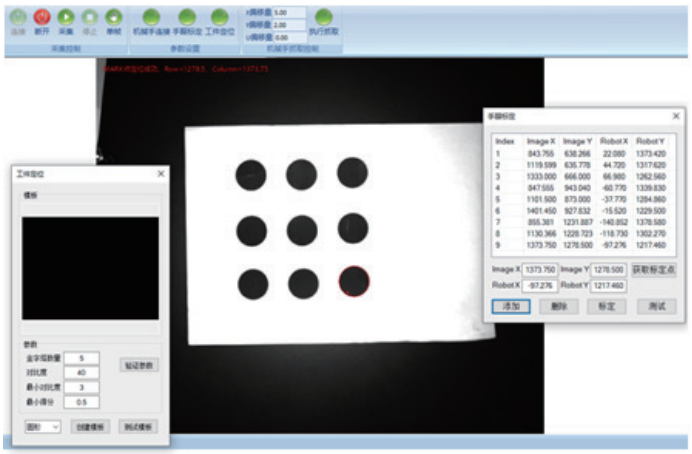

Fig. 7. (Color online) Software interface for evaluation of calibration.

Table 2
Experimental pairs of coordinates for calibration.

Data No.	1	2	3	4	5	6	7	8	9
u	843.755	1119.599	1333.000	847.555	1101.500	1401.450	855.381	1130.366	1373.750
v	638.266	635.778	666.000	943.040	873.000	927.832	1231.887	1228.723	1278.500
X_W	22.080	44.720	66.980	−60.770	−37.770	−15.520	−140.852	−118.730	−97.276
Y_W	1373.420	1317.620	1262.560	1339.830	1284.860	1229.500	1378.580	1302.270	1217.460

By substituting the pairs of coordinates in Table 2 into Eq. (9) and solving Eq. (10), the homograph matrix $\boldsymbol{H}$ of the camera model applied in the spindle positioning system of the grinding-wheel-saw automatic replacement system is evaluated to be

$$H = \begin{bmatrix} -0.274407 & -0.0882941 & 317.508 \\ -0.0360674 & 0.229713 & 1075.89 \\ 0 & 0 & 1 \end{bmatrix}. \tag{11}$$

5. Spindle Location Detection via Template Matching Approach

In the proposed grinding-wheel-saw automatic replacement system, the key issue is to detect the location of the hexagonal shaft nut on the spindle. Machine vision is the main technology used to achieve high detection accuracy for the identification of an object and its orientation. In the literature, the most commonly applied methods for object detection have been template matching methods[25–28] and feature-point matching methods.[29,30] Because the shaft nut on the spindle of the round bar sawing equipment is hexagonal and symmetric, the developed template matching approach is applied in this work. The template matching is implemented on the basis of the similarity between images, and realized by finding the area closest to the target template in the obtained image. The principle of template matching is to make a template image and then slide it in the original image. By evaluating the defined scores of similarity for the template image with the original image, it can be determined whether specific areas are similar or the same.

In a workshop, the spindle nut of a grinding-wheel saw may be coated with metal dust and high-temperature metal shavings due to the high rotation speed of the grinding-wheel saw. It is found that the quality of the directly acquired image of the spindle nut is poor. Directly applying such an acquired image to the template matching procedure will result in the failure of spindle localization. Therefore, the image captured by the digital camera must be treated before the template matching procedure. The processes for positioning the shaft nut of the spindle by machine vision include image acquisition, filtering, and enhancement and template matching.

5.1 Image acquisition, filtering, and enhancement

The shaft nut of the spindle is located at the center position of the grinding-wheel saw. It is not necessary to capture images of the shaft nut by the digital camera successively. When the main control system is giving commands for spindle localization, one image of the spindle nut of

the grinding-wheel saw is captured by the digital camera. However, the edge and contour of the acquired image of the spindle nut must be clear and smooth. Therefore, pre-processing of the image is carried out. The guided filtering algorithm[31,32] is utilized to effectively preserve edges and remove noises. In addition, to emphasize the local characteristics of the spindle nut image, improve the image quality, and strengthen the effect of recognition for template matching, image enhancement,[33,34] such as enhancement of the contrast and brightness of the image, is adopted. The experimental results for image pre-processing are illustrated in Fig. 8.

5.2 Template matching

The main object to be detected is the hexagonal shaft nut in the circular part of the grinding-wheel saw. Firstly, a reference image is taken and gray processing is carried out in sequence to build a standard template. The circular center of the shape feature of the shaft nut of the spindle is recorded. Then, the testing image is acquired and gray processing is performed for the template matching operation. The final results of the template matching can provide the (X_W, Y_W) coordinates of the center and the rotational angle of the hexagonal shaft nut in the world frame. The obtained coordinates are the motion commands and are transferred to the robot arm controller by Ethernet.

In this work, the template matching with a suitable algorithm is realized by C# language programming with the MVTec HALCON 18.11 machine-vision library. There are five main steps included in the template matching to achieve object detection. The details are described in the following, and the experimental results of the template matching operation are shown in Fig. 9.

Step 1 For the pre-processing image, an area including the shaft nut is circled and gray processing of the image is performed to set up the region of interest (ROI).

Step 2 The image template of the shaft nut is obtained by clipping the ROI.

Step 3 The image pyramid construction[35,36] of the image template is created.

Step 4 The shape template model of the shaft nut is created.

Step 5 The testing image is subjected to gray processing, then template matching with the least-squares algorithm. The matching results are analyzed and the center coordinates and rotational angle of the shaft nut are output.

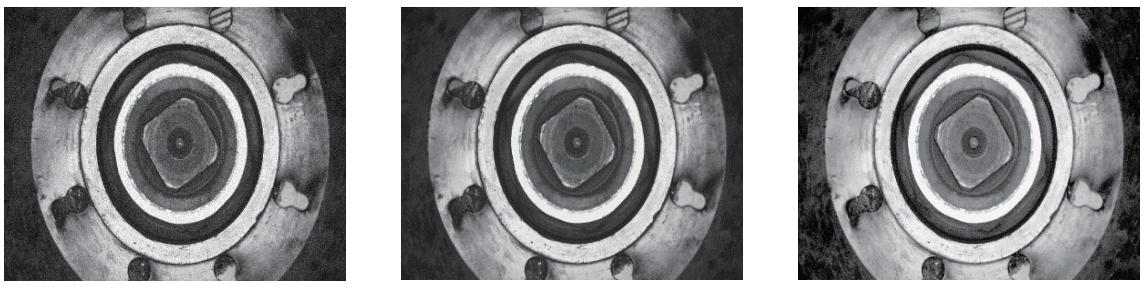

(a) (b) (c)

Fig. 8. Experimental results for image pre-processing. (a) Image acquisition. (b) Image filtering. (c) Image enhancement.

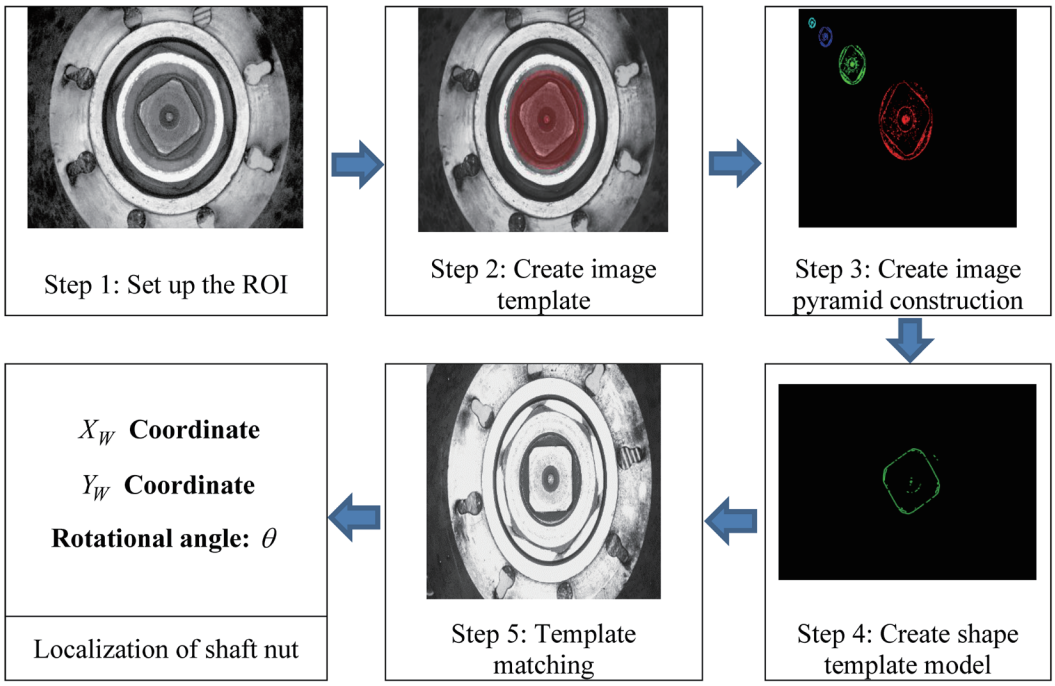

Fig. 9. (Color online) Experimental results of template matching.

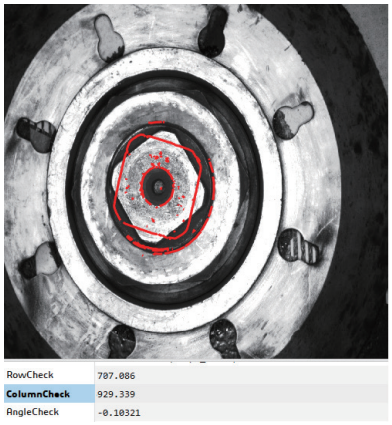

Fig. 10. (Color online) Results of machine-vision-based detection.

To evaluate the identification of the shaft nut of the spindle by the proposed machine-vision system, the experimental results are obtained. The software interface is depicted in Fig. 10. The machine-vision-based detected coordinates of the center and the rotational angle of the hexagonal shaft nut are

$$X_W = 707.086 \text{ mm}, \; Y_W = 020.339 \text{ mm}, \text{ and } \theta = -0.10321°.$$

By testing the whole steel round bar sawing equipment with the saw replacement system set up in the workshop, we found that the developed machine-vision-based spindle positioning

system can accurately locate the position of the hexagonal shaft nut of the spindle. Thus, the grinding-wheel-saw automatic replacement system can indeed replace grinding-wheel saws. Compared with 30 min taken for the manual replacement, the automatic replacement system with the machine-vision-based positioning system can complete the whole process of changing saws within 8 min.

Currently, most grinding-wheel machines with machine-vision systems are applied to polish the rough surface of a manufacturing workpiece,[3,7] and grinding-wheel equipment with machine-vision parts for sawing has seldom been set up. The established machine-vision-based spindle positioning system is suitable for grinding-wheel-saw equipment with a huge saw and greatly improves its operational efficiency and precision.

6. Conclusions

In this work, a machine-vision-based spindle positioning system for a grinding-wheel-saw automatic replacement system has been developed. The setup of the hardware and software for the vision system was reported and the imaging model of the camera and the calibration of the vision system were introduced. The template matching procedures for the localization of the hexagonal shaft nut of the spindle were also described. Experimental results demonstrated the effectiveness of the proposed machine-vision-based system.

Acknowledgments

This work was carried out as part of the Innovation Team in Green Forming Intelligent Equipment of Sanming University with financial support from the Science and Technology Department of Fujian Province (Grant No. 2020S2002), the Science and Technology Pilot Project of Sanming City (Grant No. 2019-G-11), and the Operational Funding of the Advanced Talents for Scientific Research (19YG04) of Sanming University. The authors also acknowledge the support from the School of Mechanical and Electric Engineering, Sanming University.

References

1 X. Q. Xiong and X. J. Wang: Intel. Computer Appl. **10** (2020) 111. https://doi.org/10.3969/j.issn.2095-2163.2020.02.023
2 J. Zhao, H. T. Zhu, J. P. Qu, and G. L. Zhang: Transducer Micro. Technol. **32** (2013) 139. https://doi.org/10.13873/j.1000-97872013.11.032
3 C. H. Lee, J. S. Jwo, H. Y. Hsieh, and C. S. Lin: IEEE Access **8** (2020) 58279. https://doi.org/10.1109/ACCESS.2020.2982800
4 Q. X. You, Q. W. Zhao, Y. X. Chen, and Y. Q. Li: Transducer Micro. Technol. **38** (2019) 29. https://doi.org/10.13873/J.1000-9787(2019)12-0029-04
5 N. Qiao, K. Xiao, and C. Wei: Recent Adv. Electr. Electron. Eng. **11** (2018) 457. https://doi.org/10.2174/2352096511666180213115737
6 N. Banafian, R. Fesharakifard, and M. B. Menhaj: Int. J. Adv. Manuf. Technol. **114** (2021) 251. https://doi.org/10.1007/s00170-021-06782-4
7 Z. Fang, J. Li, and C. Zhang: Int. J. Adv. Manuf. Technol. **111** (2020) 1471. https://doi.org/10.1007/s00170-020-06125-9
8 G. O. Tysse, A. C. Member, and O. Egeland: IEEE/ASME T. Mechatron. **26** (2021) 416. https://doi.org/10.1109/TMECH.2020.3024637

9 M. Faisal, M. Alsulaiman, M. Arafah, and M. A. Mekhtiche: IEEE Access **8** (2020) 167985. https://doi.org/10.1109/ACCESS.2020.3023894
10 J. Wan, S. Tang, D. Li, M. Imran, C. Zhang, C. Liu, and Z. Pang: IEEE T. Ind. Inform. **15** (2019) 507. https://doi.org/10.1109/TII.2018.2843811
11 L. Deng, G. Lu, Y. Shao, M. Fei, and H. Hu: Neurocomputing **174** (2016) 456. https://doi.org/10.1016/j.neucom.2015.03.119
12 W. Huang and N. Liu: Int. J. Computer Technol. **4** (2017) 27.
13 I. Enebuse, M. Foo, B. K. K. Ibrahim, H. Ahmed, F. Supmak, and O. S. Eyobu: IEEE Access **9** (2021) 113143. https://doi.org/10.1109/ACCESS.2021.3104514
14 D'A. Luigi, G. Emanuele, M. Pietro, and P. Paolo: Mach. Vision Appl. **32** (2021) 90. https://doi.org/10.1007/s00138-021-01219-0
15 C. Garcia: Auton. Robot. **6** (1999) 223. https://doi.org/10.1023/A:1008891612854
16 M. Fiala and C. Shu: Mach. Vision Appl. **19** (2008) 209. https://doi.org/10.1007/s00138-007-0093-z
17 K. Guo, H. Ye, J. Gu, and H. Chen: Appl. Sci-Basel. **11** (2021) 6014. https://doi.org/10.3390/app11136014
18 C. Lu: IEEE T. Pattern Anal. **22** (2000) 610. https://doi.org/10.1109/34.862199
19 P. S. Adrian, A. C. Juan, and M.N. Francesc: IEEE T. Pattern Anal. **35** (2013) 2387. https://doi.org/10.1109/TPAMI.2013.36
20 X. X. Lu: J. Phys. Conf. Series **1087** (2018) 052009. https://doi.org/10.1088/1742-6596/1087/5/052009
21 B. Zhou, Z. Chen, and Q. Liu: IEEE Access **8** (2020) 162838. https://doi.org/10.1109/ACCESS.2020.3021313
22 D. Oberkampf, D. DeMenthon, and L. Davis: Computer Vision Imag. Und. **63** (1996) 495. https://doi.org/10.1006/cviu.1996.0037
23 Z. Y. Zhang: IEEE T. Pattern Anal. **22** (2000) 1330. https://doi.org/10.1109/34.888718
24 G. Schweighofer and A. Pinz: IEEE T. Pattern Anal. **28** (2006) 2024. https://doi.org/10.1109/TPAMI.2006.252
25 C. F. Zhao, H. C. Ding, G. H. Cao, and H. Han: Adv. Mech. Eng. **13** (2021) 1. https://doi.org/10.1177/16878140211034616
26 S. C. Wang, H. Wang, Y. L. Zhou, J. B. Liu, P. Dai, X. Y. Du, and W. M. Abdel: Measurement **169** (2021) 108362. https://doi.org/10.1016/J.MEASUREMENT.2020.108362
27 J. Sato, T. Yamada, K. Ito, and T. Akashi: IEEJ T. Electr. Electron. Eng. **16** (2020) 117. https://doi.org/10.1002/TEE.23274
28 F. Chen, J. Liao, and Z. Lu: Pattern Anal. Appl. **24** (2021) 1427. https://doi.org/10.1007/s10044-021-00997-7
29 J. Y. Shen, X. C. Guo, W. Z. Zhou, Y. M. Zhang, and J. C. Li: Symmetry **13** (2021) 407. https://doi.org/10.3390/SYM13030407
30 K. Tomasz, S. Piotr, R. Tomasz, R. Pawel and S. Zygmunt: Sensors **20** (2020) 2401. https://doi.org/10.3390/s20082401
31 K. He, J. Sun, and X. Tang: IEEE T. Pattern Anal. **33** (2011) 2341. https://doi.org/10.1109/TPAMI.2010.168
32 Q. S. Zhu, J. M. Mai, and L. Shao: IEEE T. Imag. Process. **24** (2015) 3522. https://doi.org/10.1109/TIP.2015.2446191
33 J. S. Lee: IEEE T. Pattern Anal. **2** (1980) 165. https://doi.org/10.1109/TPAMI.1980.4766994
34 M. Irani and S. Peleg: J. Vis. Commun. Imag. R. **4** (1993) 324. https://doi.org/10.1006/jvci.1993.1030
35 Z. J. Jiang and H. A. Yi: Geo. Inf. Sci. Wunan Univ. **32** (2007) 680. https://doi.org/10.3969/j.issn.1671-8860.2007.08.006
36 K. Ren, L. Meng, and G. U. Zeling: Chin. Measure. Test **44** (2018) 83. https://doi.org/10.11857/j.issn.1674-5124.2018.07.016